The global population of SARS-CoV-2 is composed of six major subtypes

Ivair José Morais Júnior[ad], Richard Costa Polveiro[b], Gabriel Medeiros Souza[a], Daniel Inserra Bortolin[a], Flávio Tetsuo Sassaki[c], Alison Talis Martins Lima[a#]

[a]Instituto de Ciências Agrárias/Universidade Federal de Uberlândia, Uberlândia, MG 38410-337, Brazil

[b]Departamento de Veterinária/Universidade Federal de Viçosa, Viçosa, MG 36570-900, Brazil

[c]Instituto de Biotecnologia/Universidade Federal de Uberlândia, Monte Carmelo, MG 38500-000, Brazil

[d]Current address: Departamento de Fitopatologia/Universidade de Brasília, Brasília, DF 73345-010, Brazil

#Corresponding author: Alison Talis Martins Lima

Phone: (+55-34) 2512-6716; E-mail: atmlima@ufu.br

Abstract

The World Health Organization characterized the COVID-19 as a pandemic in March 2020, the second pandemic of the 21st century. Severe acute respiratory syndrome coronavirus 2 (SARS-CoV-2) is a positive-stranded RNA betacoronavirus of the family *Coronaviridae*. Expanding virus populations, as that of SARS-CoV-2, accumulate a number of narrowly shared polymorphisms imposing a confounding effect on traditional clustering methods. In this context, approaches that reduce the complexity of the sequence space occupied by the SARS-CoV-2 population are necessary for a robust clustering. Here, we proposed the subdivision of the global SARS-CoV-2 population into sixteen well-defined subtypes by focusing on the widely shared polymorphisms in nonstructural (*nsp*3, *nsp*4, *nsp*6, *nsp*12, *nsp*13 and *nsp*14) cistrons, structural (*spike* and *nucleocapsid*) and accessory (*ORF8*) genes. Six virus subtypes were predominant in the population, but all sixteen showed amino acid replacements which might have phenotypic implications. We hypothesize that the virus subtypes detected in this study are records of the early stages of the SARS-CoV-2 diversification that were randomly sampled to compose the virus populations around the world, a typical founder effect. The genetic structure determined for the SARS-CoV-2 population provides substantial guidelines for maximizing the effectiveness of trials for testing the candidate vaccines or drugs.

Main

In December 2019, a local pneumonia outbreak of initially unknown etiology was detected in Wuhan (Hubei, China) and quickly determined to be caused by a novel coronavirus[1], named severe acute respiratory syndrome coronavirus 2 (SARS-CoV-2)[2] and the disease as COVID-19[3]. SARS-CoV-2 is classified in the family *Coronaviridae*, genus *Betacoronavirus*, which comprises enveloped, positive stranded RNA viruses of vertebrates[2]. Two-thirds of SARS-CoVs genome is covered by the ORF1ab, that encodes a large polypeptide which is cleaved into 16 nonstructural proteins (NSPs) involved in replication-transcription in vesicles from endoplasmic reticulum (ER)-derived membranes[4,5]. The last third of the virus genome encodes four essential structural proteins: spike (S), envelope (E), membrane (M), nucleocapsid (N) and several accessory proteins that interfere with the host innate immune response[6].

Populations of RNA viruses evolve rapidly due to their large population sizes, short generation times, and high mutation rates of viruses, this latter is a consequence of the RNA-dependent RNA polymerase (RdRP) which lacks the proofreading activity[7]. In fact, virus populations are composed of a broad spectrum of closely related genetic variants resembling one or more master sequences[8–10]. Mutation rates inferred for SARS-CoVs are considered moderate[11,12] due to the independent proofreading activity[13]. However, the large SARS-CoV genomes (from 27 to 31 kb)[14] provide to them the ability to explore the sequence space[15]. In order to better understand the diversification of SARS-CoV-2 genomes during the pandemics (from December 2019 to March 25, 2020), we applied a simple, but robust approach to reduce the complexity of the sequence space occupied by the virus population by detecting its widely shared polymorphisms.

The 767 SARS-CoV-2 genomes with high sequencing coverage obtained from GISAID (https://www.gisaid.org/) and GenBank were clustered into 593 haplotypes (Supplementary Table 1). We conducted a fine-scale sequence variation analysis on the 593 genomes-containing alignment by calculating the nucleotide diversity (π) using a sliding window and step size of 300 and 20 nucleotides, respectively (multiple sequence alignments generated in this study are available from the authors upon request). Such an approach allows to identify genomic regions of increased genetic variation prevenient from polymorphic sites harboring two or more distinct nucleotide bases. Noticeably, one or more large clusters of closely related sequences, when analyzed by this approach, show locally increased nucleotide diversity. We observed a contrasting distribution of the genetic variation across the full-length genomes of SARS-CoV-2 (Figure 1) with eight segments showing increased genetic

variation, arbitrarily defined as nucleotide (nt) segments with $\pi \geq 0.001$ (Table 1). Seven out of eight segments had about 280 nucleotides in length, corresponding approximately to the size of a single sliding window, except the S10 whose length was equivalent to two sliding windows (600 nt). To further investigate the diversification of segments with contrasting content of genetic variability, we constructed maximum likelihood (ML) phylogenetics trees and analyzed the diversification patterns of eight segments with higher (S2, 4, 6, 8 10, 12, 14 and 16), and nine with lower (S1, 3, 5, 7, 9, 11, 13, 15 and 17) content of genetic variation, respectively (the ML analyses were used in this study essentially as a clustering method due to the weak phylogenetic signal in the data set).

Although the data set was composed of hundreds of SARS-CoV-2 genomes sampled from around the world, in the S2-based tree we observed two clusters (Figure 2). Markedly, each cluster was composed of very closely related, if not identical, sequences. Therefore, the increased content of genetic variation at the S2 was a result of the inter-cluster sequence comparisons. Similar results were obtained for the other seven ML-trees based on segments with increased genetic variation (Supplementary Figure 1). In contrast, the ML-trees based on segments with lower content of genetic variation did not show a consistent number of well-defined clusters (Supplementary Figure 2).

We mapped the polymorphic sites in segments whose trees showed two well-defined clusters (Table 1). Only a few (from one to three) nt positions with polymorphisms shared by a number of SARS-CoV-2 genomes could be identified within each segment with increased genetic variation. These polymorphisms were henceforth referred to as ‘widely shared polymorphisms’ (WSPs), while the remaining nt sites in virus genomes were designed as ‘non widely shared polymorphisms’ (nWSPs).

We compared the topologies of the seventeen ML-trees (eight based on WSPs-containing segments and nine based on segments with nWSPs, Supplementary Figures 1 and 2, respectively). The topology of trees based on WSPs-containing segments was considerably congruent indicating a frequent, but not strict, co-segregation of nt at WSPs. For example, the SARS-CoV-2 reference isolate (GISAID accession ID: EPI_ISL_402124, GenBank accession: MN908947) was placed in an equivalent major cluster in all WSPs-containing segments-based ML-trees. In contrast, the isolate EPI_ISL_416036 was placed in an equivalent minor cluster for S2, S8, S12 and S16-based ML-trees and in the major cluster for S4, S6, S10 and S14-based ML-trees. On the contrary, the topology of those ML-trees based on segments with nWSPs were highly incongruent suggesting that such regions represent a wide mutant spectrum of narrowly shared polymorphisms. It is important to note that there

are minor clusters in nWSPs-containing segments-based ML-trees, *e.g.*, in those for S1, S13 and S17. This is a consequence of our conservative threshold in which we focused on segments with $\pi \geq 0.001$. S1, S13 and S17 also show locally increased genetic variation with π higher than 0.0005 but lower than 0.001. For example, stretches 889 - 1,169; 1,409 - 1,509 (within the S1); 25,403 - 25,693 (S13); 29,538 - 29,610 (S17).

Therefore, our approach reduced the complexity of the sequence space occupied by the SARS-CoV-2 genomes and provided a robust clustering solution based on the combination of 12 WSPs (Table 1) to identify the major viral genotypes spread worldwide (Figure 3). The global population of SARS-CoV-2 is structured into six major subtypes (I - VI), comprising 578 out of 593 (about 97.5%) isolates analyzed in this study. The Subtype I (N=132) was represented by the combination of the most frequent nucleotides at all WSPs, *i.g.*, the canonical genotype: CCGCCACAUGGG. The SARS-CoV-2 reference isolate is a representative member of this subtype. Subtype IV (N=91) was represented by the combination of the most frequent nucleotides at eleven out of 12 WSPs (**CC**U**CCACAUGGG**; the most frequent nucleotides at each WSP are highlighted in bold and underlined). Subtypes V (N=74, **C**U**GCCACA**C**GGG**), II (N=122, U**CG**U**CAC**G**UGGG**), III (N=101, **C**U**GC**UGU**A**C**GGG**) and VI (N=58, U**CG**U**CAC**G**U**AAC) were represented by the combination of the most frequent nucleotides at ten, nine, seven and six out of 12 WSPs, respectively. It is important to emphasize that the contrasting sample sizes (Subtypes I - IV *vs.* VII - XVI) are not necessarily associated with fitness variation and might be due to a sampling bias. For example, the three isolates composing the Subtype VIII showed a genotype (**C**U**GCCA**U**ACGGG**) very similar to that of the canonical reference isolate. In addition, even though our data set was composed exclusively by genomes with high sequencing coverage, we cannot rule out that the virus subtypes X to XVI, which were represented by a single genome might be a consequence of poor sampling or sequencing errors.

The phylogenetic tree depicting all 593 SARS-CoV-2 haplotypes showed some geographical structure with two clusters: a smaller one comprised of isolates mostly sampled from Western hemisphere (Subtypes II, VI, IX, X and XI) and a larger one whose isolates were sampled from Western and Eastern hemispheres (I, III, IV, V, VII, VIII, XII, XIII, XIV, XV and XVI).

We hypothesize that our clustering method for the SARS-CoV-2 population could involve at some extent a biological context. Nine out of 12 WSPs led to amino acid replacements (Table 2), *e.g.*, the WSP *nsp*6-[111] in nine SARS-CoV-2 subtypes led to a leucine at the aa residue#37 of the protein and a phenylalanine in seven other subtypes. NSP6 is an integral membrane protein that interferes in

the autophagosome formation during the SARS-CoV infection. Additionally, in yeast two-hybrid experiments, NSP6 has been shown to interact with NSP3[16]. Some evidence demonstrates that NSP6 protein limits the expansion of autophagosomes or, alternatively, might remove host proteins involved in inhibition of viral replication by activating autophagy from the ER[17].

The WSP *nsp*12-[967] resulted in a proline in eleven subtypes of SARS-CoV-2 and a leucine in others five subtypes at the aa residue #323 of the NSP12 (RNA-dependent RNA polymerase, RdRP) protein. It is located at the Interface domain of RdRP of SARS-CoV-2, which is responsible for the connection between the nidovirus RdRP-associated nucleotidyltransferase domain (NiRAN) and the "Right hand" polymerase domain[18]. The S protein mediates viral entry into host cells by first binding to a receptor, angiotensin-converting enzyme 2 (ACE2), through the receptor-binding domain (RBD) in the S1 subunit and then fusing the viral and host membranes through the S2 subunit[19–22]. Sites of glycosylation are important for S protein folding[23], affecting priming by host proteases[24] and might modulate antibody recognition[25,26]. The WSP *S*-[1,841] resulted in a glycine and an aspartate at the aa residue#614 of the S protein in six and ten subtypes of SAR-CoV-2, respectively. The replacement was mapped in the intermediate region between the S1 and S2 subunits. This WSP is near a glycosylation site (N616CT)[27].

The WSP *ORF8*-[251] involved a non-synonymous mutation at the codon#84 encoding for leucine and serine in nine and seven subtypes, respectively. The SARS-CoV ORF8 encodes for an ER-associated protein that induces the activation of ATF6, and this latter is an ER stress-regulated transcription factor that stimulates the production of chaperones[28]. In addition, the ORF8 protein has been demonstrated to induce apoptosis[29]. In SARS epidemics, the *ORF8* from different coronaviruses was targeted by a number of mutations and recombination events during transmission from animals to humans[30].

Three WSPs mapped in the *N* gene led to two amino acid replacements at residues#203 and #204. The multifunctional N protein is composed of three domains[31], two of which are structurally independent: the N-terminal domain (NTD) and the C-terminal domain (CTD). Both amino acid replacements were mapped in an intermediary domain referred to as the linker region (LKR), a positively charged serine-arginine-rich region. As an intrinsically disordered region (IDR) it allows the independent folding of the NTD and CTD[32] and is also functionally implicated in RNA binding activity[31]. Key determinants of the interaction between the N and NSP3 proteins were also mapped at the LKR[33]. The SARS-CoV N protein is also responsible for an antigenic response in humans

158 predominantly involving the immunoglobulin G[34] (the three-dimensional protein maps highlighting
159 the amino acid replacements are available as Supplementary Figure 3). Although the host biological
160 factors involved in the response to SARS-CoV-2 infection are still poorly known, the existence of
161 distinct virus subtypes, all of them exhibiting amino acid replacements, could alter important aspects
162 of COVID-19.

163 We hypothesized that in the early stages of the SARS-CoV-2 epidemics, due to the rapid virus
164 population expansion, a number of genetic variants might have arisen followed by a spread of non-
165 representative sampling of variants to other countries and continents, *i.g.*, a founder effect. We argue
166 that the virus subtypes and their associated WSPs detected in this study would be records of
167 diversification in these early stages of the epidemics after transmission from animal to humans. After
168 the virus introduction in a given geographic region, a number of unique or narrowly shared mutations
169 is accumulated, however, most of them reduce the fitness and are removed by purifying selection in a
170 medium to long term evolutionary scale, tending to a decreasing genetic variability[8].

171 We propose a classification into at least sixteen distinct subtypes of SARS-CoV-2, six of them
172 accounting for more than 97% of the sampled isolates from around the world. Such classification
173 might guide the validation of candidate vaccines or drugs for the widest range of virus subtypes. In
174 this context, our clustering solution provides a robust approach to effectively reduce the complexity
175 of the mutant spectrum composed of closely related SARS-CoV-2 genomes focusing on WSPs.
176 Additionally, through the exhaustive sequencing, it would be possible to identify novel virus subtypes
177 and follow the evolutionary dynamics of the SARS-CoV-2 population during the adaptive process
178 imposed by the human host.

179 **Table 1.** Characterization of the WSPs detected in genomes of SARS-CoV-2
180

Segment ID	Segment position* (begin - end)	WSPs†	nt mutation (# isolates)	Position in the codon	#codon	Amino acid
S2	2,872 - 3,152	*nsp*3-[318]	**U** (184) / **C** (409)	Third	106	Phenylalanine/Phenylalanine
S4	8,612 - 8,892	*nsp*4-[228]	**U** (183) / **C** (410)	Third	76	Serine/Serine
S6	10,932 - 11,192	*nsp*6-[111]	**C** (1) / **U** (99) / **G** (493)	Third	37	Phenylalanine/Phenylalanine/Leucine
S8	14,232 - 14,512	*nsp*12-[967]	**U** (184) / **C** (409)	Second	323	Leucine/Proline
S10	17,573 -18,173	*nsp*13-[1,511]	**U** (101) / **C** (492)	Second	504	Leucine/Proline
		*nsp*13-[1,622]	**G** (101) / **A** (492)	Second	541	Cysteine/Tyrosine
		*nsp*14-[21]	**U** (105) / **C** (488)	Third	7	Leucine/Leucine
S12	23,243 - 23,523	*S*-[1,841]	**G** (185) / **A** (408)	Second	614	Glycine/Aspartate
S14	27,977 - 28,258	*ORF*8-[251]	**C** (184) / **U** (409)	Second	84	Serine/Leucine
S16	28,718 - 28,998	*N*-[608]	**A** (60) / **G** (533)	Second	203	Lysine/Arginine
		N-[609]	**A** (60) / **G** (533)	Third		
		N-[610]	**C** (60) / **G** (533)	First	204	Glycine/Arginine

181 *Relative to the multiple sequence alignment constructed for full-length genomes
182 †Widely Shared Polymorphisms (WSPs) are conventionally indicated by *cistron*/*gene*-[nt position within the cistron or gene]

Table 2. Amino acid composition of each virus subtype at WSP positions

SUBTYPE	N*	WSP POSITION											
		nsp3	*nsp4*	*nsp6*	*nsp12*	*nsp13*		*nsp14*	*S*	*ORF8*	*N*		
		#318	#228	#111	#967	#1511	#1622	#21	#1,841	#251	#608	#609	#610
I	132	C [Phe]†	C [Ser]	G [Leu]	C [Pro]	C [Pro]	A [Tyr]	C [Leu]	A [Asp]	U [Leu]	G [Arg]	G [Arg]	G [Arg]
II	122	U [Phe]	C [Ser]	G [Leu]	U [Leu]	C [Pro]	A [Tyr]	C [Leu]	G [Gly]	U [Leu]	G [Arg]	G [Arg]	G [Arg]
III	101	C [Phe]	U [Ser]	G [Leu]	C [Pro]	U [Leu]	G [Cys]	U [Leu]	A [Asp]	C [Ser]	G [Arg]	G [Arg]	G [Arg]
IV	91	C [Phe]	C [Ser]	U [Phe]	C [Pro]	C [Pro]	A [Tyr]	C [Leu]	A [Asp]	U [Leu]	G [Arg]	G [Arg]	G [Arg]
V	74	C [Phe]	U [Ser]	G [Leu]	C [Pro]	C [Pro]	A [Tyr]	C [Leu]	A [Asp]	C [Ser]	G [Arg]	G [Arg]	G [Arg]
VI	58	U [Phe]	C [Ser]	G [Leu]	U [Leu]	C [Pro]	A [Tyr]	C [Leu]	G [Gly]	U [Leu]	A [Lys]	A [Lys]	C [Gly]
VII	3	C [Phe]	U [Ser]	U [Phe]	C [Pro]	C [Pro]	A [Tyr]	C [Leu]	A [Asp]	C [Ser]	G [Arg]	G [Arg]	G [Arg]
VIII	3	C [Phe]	U [Ser]	G [Leu]	C [Pro]	C [Pro]	A [Tyr]	U [Leu]	A [Asp]	C [Ser]	G [Arg]	G [Arg]	G [Arg]
IX	2	U [Phe]	C [Ser]	U [Phe]	U [Leu]	C [Pro]	A [Tyr]	C [Leu]	G [Gly]	U [Leu]	A [Lys]	A [Lys]	C [Gly]
X	1	U [Phe]	C [Ser]	U [Phe]	U [Leu]	C [Pro]	A [Tyr]	C [Leu]	G [Gly]	U [Leu]	G [Arg]	G [Arg]	G [Arg]
XI	1	U [Phe]	C [Ser]	G [Leu]	C [Pro]	C [Pro]	A [Tyr]	C [Leu]	G [Gly]	U [Leu]	G [Arg]	G [Arg]	G [Arg]
XII	1	C [Phe]	U [Ser]	C [Phe]	C [Pro]	C [Pro]	A [Tyr]	C [Leu]	A [Asp]	C [Ser]	G [Arg]	G [Arg]	G [Arg]
XIII	1	C [Phe]	C [Ser]	G [Leu]	C [Pro]	C [Pro]	A [Tyr]	C [Leu]	A [Asp]	C [Ser]	G [Arg]	G [Arg]	G [Arg]
XIV	1	C [Phe]	U [Ser]	G [Leu]	C [Pro]	C [Pro]	A [Tyr]	C [Leu]	G [Gly]	C [Ser]	G [Arg]	G [Arg]	G [Arg]
XV	1	C [Phe]	C [Ser]	U [Phe]	U [Leu]	C [Pro]	A [Tyr]	C [Leu]	A [Asp]	U [Leu]	G [Arg]	G [Arg]	G [Arg]
XVI	1	C [Phe]	C [Ser]	U [Phe]	C [Pro]	C [Pro]	A [Tyr]	U [Leu]	A [Asp]	U [Leu]	G [Arg]	G [Arg]	G [Arg]

*Sample size

#Nucleotide position

†Nucleotide base and the encoded amino acid residue

188 **Figure legends**

189 **Figure 1.** Mean pairwise number of nucleotide differences per site (nucleotide diversity, π)
190 calculated using a sliding window of 300 nucleotides across the multiple sequence alignment for
191 full-length genomes of SARS-CoV-2. The red dashed line at $\pi = 0.001$ represents an arbitrary
192 threshold to subdivide the segments (S) with increased (S2, 4, 6, 8, 10, 12, 14 and 16) and lower
193 (S1, 3, 5, 7, 9, 11, 13,15 and 17) content of genetic variation. The SARS-CoV-2 genome
194 organization is represented on top of the plot.

195 **Figure 2.** Maximum likelihood phylogenetic tree based on a nucleotide sequence between the
196 positions 2,872 - 3,152 (S2) of the aligned SARS-CoV-2 genomes.

197 **Figure 3.** Maximum likelihood phylogenetic tree based on 12 WSPs detected across the SARS-
198 CoV-2 genomes.

199

Methods

A total of 1,137 full-length genomes of SARS-CoV-2 sampled from December 2019 to March 25, 2020 (at 2:30 pm) were obtained from Genbank[35] and GISAID[36] (Supplementary Table S1). Only genomes with high sequencing coverage, intact ORFs (no frameshifts, except that of *nsp*12 cistron) and without any indeterminate nucleotide base (indicated by 'N's or ambiguous codes) totalizing 767 high quality full-length sequences were effectively analyzed in this study.

The genomic data set was aligned using MAFFT-FFT-NS-2[37]. The calculation of the average number of nucleotide differences per site (nucleotide diversity, π) was conducted in DnaSP v.6[38] using a sliding window and step size of 300 and 20 nucleotides, respectively. Sites with gaps alignment were not considered in analysis. The detection of polymorphic sites was conducted using PAUP* v. 4.0[39] and MEGA X[40]. Those sites responsible for the segregation of the isolates into two clusters in the ML-trees were referred to as "widely shared polymorphisms" (WSPs), while the remaining nt sites in the virus genomes were designed as "non widely shared polymorphisms" (nWSPs). The WSPs were conventionally indicated by *cistron/gene* name-[nt position within the cistron or gene]. We opted by indicating the nt position within the cistron or gene due to their highly conserved sizes (no gap was introduced during the construction of sequence alignments), in contrast to the full-genomes whose 5'- and 3'-untranslated regions (UTRs) were highly variable in terms of length.

Maximum likelihood (ML) phylogenetic trees were constructed using RAxML[41] under the nucleotide substitution model General Time-Reversible with gamma distribution (GTRGAMMA). The branch support for ML-trees based on WSPs-containing and nWSPs segments was assessed with 1,000 and 5,000 bootstrap replications, respectively. All phylogenetic trees were edited using iTOL[42].

References

1. Wu, F. *et al.* A new coronavirus associated with human respiratory disease in China. *Nature* **579**, 265–269 (2020).
2. Coronaviridae Study Group of the International Committee on Taxonomy of Viruses. The species Severe acute respiratory syndrome-related coronavirus: classifying 2019-nCoV and naming it SARS-CoV-2. *Nat. Microbiol.* **5**, (2020).
3. WHO. WHO Director-General's remarks at the media briefing on 2019-nCoV on 11 February 2020. *WHO website* https://www.who.int/dg/speeches/detail/who-directo (2020).
4. Sawicki, S. G. & Sawicki, D. L. Coronavirus Transcription: A Perspective. in *Current topics in microbiology and immunology* vol. 287 31–55 (2005).
5. de Wilde, A. H., Snijder, E. J., Kikkert, M. & van Hemert, M. J. Host Factors in Coronavirus Replication. in *Assessment & Evaluation in Higher Education* vol. 37 1–42 (Springer International Publishing, 2017).
6. Kim, D. *et al. The architecture of SARS-CoV-2 transcriptome*. (2020) doi:10.1088/1751-8113/44/8/085201.
7. Peck, K. M. & Lauring, A. S. Complexities of Viral Mutation Rates. *J. Virol.* **92**, (2018).
8. Simmonds, P., Aiewsakun, P. & Katzourakis, A. Prisoners of war — host adaptation and its constraints on virus evolution. *Nat. Rev. Microbiol.* **17**, 321–328 (2019).
9. Domingo, E., Sheldon, J. & Perales, C. Viral Quasispecies Evolution. *Microbiol. Mol. Biol. Rev.* **76**, 159–216 (2012).
10. Domingo, E. & Perales, C. Viral quasispecies. *PLoS Genet.* **15**, 1–20 (2019).
11. Zhao, Z. *et al.* Moderate mutation rate in the SARS coronavirus genome and its implications. *BMC Evol. Biol.* **4**, 1–9 (2004).
12. Gorbalenya, A. E., Enjuanes, L., Ziebuhr, J. & Snijder, E. J. Nidovirales: Evolving the largest RNA virus genome. *Virus Res.* **117**, 17–37 (2006).
13. Ma, Y. *et al.* Structural basis and functional analysis of the SARS coronavirus nsp14–nsp10 complex. *Proc. Natl. Acad. Sci.* **112**, 9436–9441 (2015).
14. Knipe, D. M. & Howley, P. M. *Fields virology*. *Viruses and the Lung: Infections and Non-Infectious Viral-Linked Lung Disorders* (2013).
15. Forni, D., Cagliani, R., Clerici, M. & Sironi, M. Molecular Evolution of Human Coronavirus Genomes. *Trends Microbiol.* **25**, 35–48 (2017).
16. Angelini, M. M., Akhlaghpour, M., Neuman, B. W. & Buchmeier, M. J. Severe Acute Respiratory Syndrome Coronavirus Nonstructural Proteins 3, 4, and 6 Induce Double-Membrane Vesicles. *MBio* **4**, 1–10 (2013).
17. Cottam, E. M., Whelband, M. C. & Wileman, T. Coronavirus NSP6 restricts autophagosome expansion. *Autophagy* **10**, 1426–1441 (2014).
18. Gao, Y. *et al.* Structure of RNA-dependent RNA polymerase from 2019-nCoV, a major antiviral drug target. *bioRxiv* 2020.03.16.993386 (2020) doi:10.1101/2020.03.16.993386.
19. Hoffmann, M. *et al.* SARS-CoV-2 Cell Entry Depends on ACE2 and TMPRSS2 and Is Blocked by a Clinically Proven Protease Inhibitor. *Cell* 1–10 (2020) doi:10.1016/j.cell.2020.02.052.
20. Li, W. *et al.* Angiotensin-converting enzyme 2 is a functional receptor for the SARS coronavirus. *Nature* vol. 426 450–454 (2003).

21. Matsuyama, S. *et al.* Efficient Activation of the Severe Acute Respiratory Syndrome Coronavirus Spike Protein by the Transmembrane Protease TMPRSS2. *J. Virol.* **84**, 12658–12664 (2010).
22. Shulla, A. *et al.* A Transmembrane Serine Protease Is Linked to the Severe Acute Respiratory Syndrome Coronavirus Receptor and Activates Virus Entry. *J. Virol.* **85**, 873–882 (2011).
23. Rossen, J. W. A. *et al.* The Viral Spike Protein Is Not Involved in the Polarized Sorting of Coronaviruses in Epithelial Cells †. *J. Virol.* **72**, 497–503 (1998).
24. Yang, Y. *et al.* Two Mutations Were Critical for Bat-to-Human Transmission of Middle East Respiratory Syndrome Coronavirus. *J. Virol.* **89**, 9119–9123 (2015).
25. Pallesen, J. *et al.* Immunogenicity and structures of a rationally designed prefusion MERS-CoV spike antigen. *Proc. Natl. Acad. Sci. U. S. A.* **114**, E7348–E7357 (2017).
26. Walls, A. C. *et al.* Unexpected Receptor Functional Mimicry Elucidates Activation of Coronavirus Fusion. *Cell* **176**, 1026–1039 (2019).
27. Walls, A. C. *et al.* Structure, Function, and Antigenicity of the SARS-CoV-2 Spike Glycoprotein. *Cell* **180**, 1–12 (2020).
28. Sung, S.-C., Chao, C.-Y., Jeng, K.-S., Yang, J.-Y. & Lai, M. M. C. The 8ab protein of SARS-CoV is a luminal ER membrane-associated protein and induces the activation of ATF6. *Virology* **387**, 402–413 (2009).
29. Chen, C. *et al.* Open Reading Frame 8a of the Human Severe Acute Respiratory Syndrome Coronavirus Not Only Promotes Viral Replication but Also Induces Apoptosis. *J. Infect. Dis.* **196**, 405–415 (2007).
30. Cui, J., Li, F. & Shi, Z.-L. Origin and evolution of pathogenic coronaviruses. *Nat. Rev. Microbiol.* **17**, 181–192 (2019).
31. Parker, M. M. & Masters, P. S. Sequence comparison of the N genes of five strains of the coronavirus mouse hepatitis virus suggests a three domain structure for the nucleocapsid protein. *Virology* **179**, 463–468 (1990).
32. Huang, Q. *et al.* Structure of the N-Terminal RNA-Binding Domain of the SARS CoV Nucleocapsid Protein. *Biochemistry* **43**, 6059–6063 (2004).
33. Verheije, M. H. *et al.* The Coronavirus Nucleocapsid Protein Is Dynamically Associated with the Replication-Transcription Complexes. *J. Virol.* **84**, 11575–11579 (2010).
34. Leung, D. T. M. *et al.* Antibody Response of Patients with Severe Acute Respiratory Syndrome (SARS) Targets the Viral Nucleocapsid. *J. Infect. Dis.* **190**, 379–386 (2004).
35. Sayers, E. W. *et al.* GenBank. *Nucleic Acids Res.* **47**, D94–D99 (2019).
36. Shu, Y. & McCauley, J. GISAID: Global initiative on sharing all influenza data – from vision to reality. *Eurosurveillance* **22**, 2–4 (2017).
37. Katoh, K., Misawa, K., Kei-ichi, K. & Miyata, T. MAFFT: a novel method for rapid multiple sequence alignment based on fast Fourier transform. *Nucleic Acids Res.* **30**, 3059–3066 (2002).
38. Rozas, J. *et al.* DnaSP 6: DNA Sequence Polymorphism Analysis of Large Data Sets. *Mol. Biol. Evol.* **34**, 3299–3302 (2017).
39. Swofford, D. L. PAUP*: Phylogenetic Analysis Using Parsimony (*and Other Methods). (2002) doi:10.1111/j.0014-3820.2002.tb00191.x.
40. Kumar, S., Stecher, G., Li, M., Knyaz, C. & Tamura, K. MEGA X: Molecular Evolutionary Genetics Analysis across Computing Platforms. *Mol. Biol. Evol.* **35**, 1547–1549 (2018).

315 41. Stamatakis, A. RAxML version 8: a tool for phylogenetic analysis and post-analysis of large
316 phylogenies. *Bioinformatics* **30**, 1312–1313 (2014).
317 42. Letunic, I. & Bork, P. Interactive Tree Of Life (iTOL) v4: recent updates and new
318 developments. *Nucleic Acids Res.* **47**, W256–W259 (2019).

Acknowledgments

This study was financed in part by the Coordenação de Aperfeiçoamento de Pessoal de Nível Superior - Brasil (CAPES) - Finance Code 001. IJM and RCP were recipients of CNPq and CAPES doctoral fellowships, respectively. DIB was the recipient of a FAPEMIG master fellowship.

Author Contributions

ATML designed the bioinformatics analyses. IJM, ATML, RCP, GMS, DIB and FTS conducted the analyses. ATML, IJM, RCP and FTS analyzed data and results. IJM, RCP, FTS and ATML wrote the manuscript. All authors contributed to the content and writing of the Supplementary Information.

Competing interest declaration

The authors declare that they have no competing interests.

Additional information

Supplementary information is available for this manuscript.

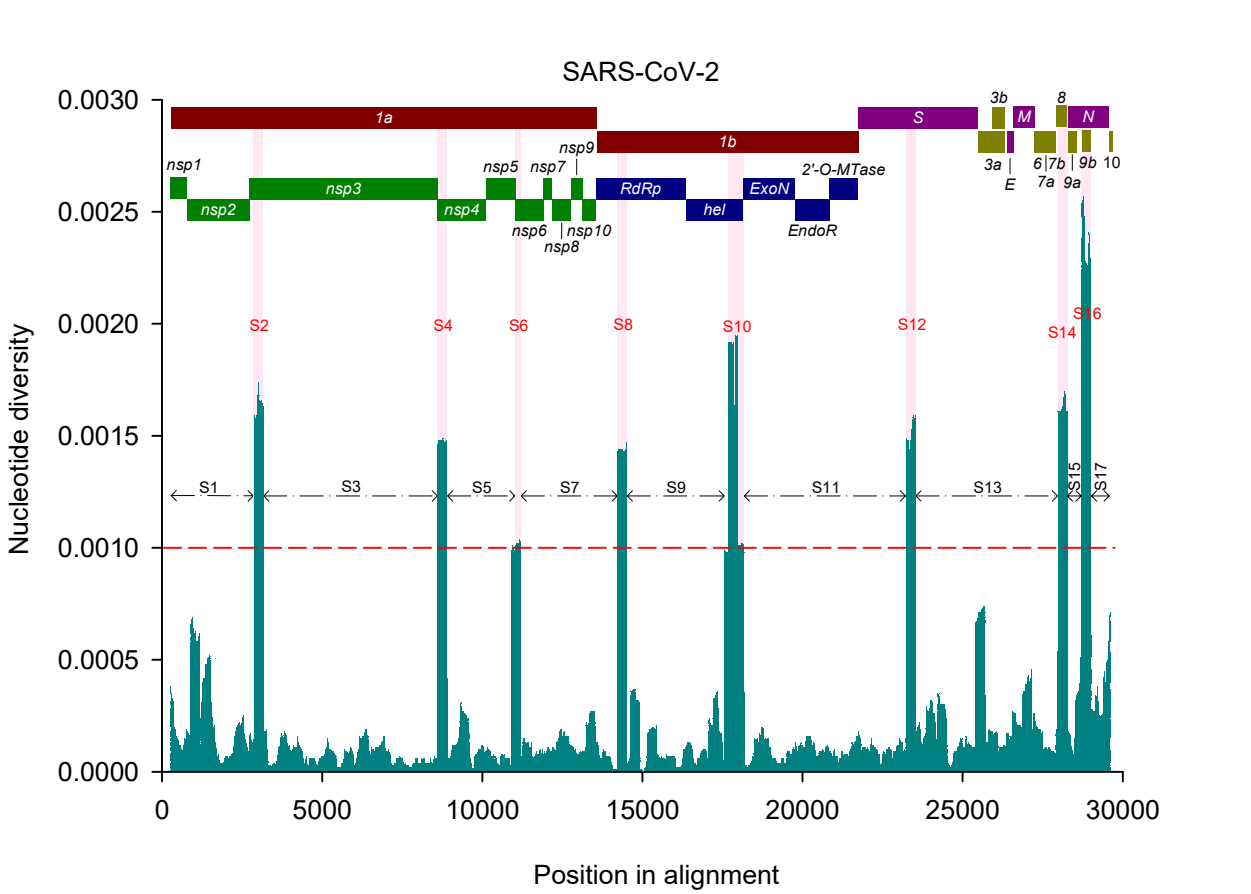
SARS-CoV-2
Nucleotide diversity
Position in alignment
0.0030
0.0025
0.0020
0.0015
0.0010
0.0005
0.0000
0
5000
10000
15000
20000
25000
30000
1a
1b
S
3b
8
M
N
nsp1
nsp2
nsp3
nsp4
nsp5
nsp6
nsp7
nsp8
nsp9
nsp10
RdRp
hel
ExoN
2'-O-MTase
EndoR
3a
E
6
7a
7b
9a
9b
10
S1
S2
S3
S4
S5
S6
S7
S8
S9
S10
S11
S12
S13
S14
S15
S16
S17

Clusters

- Major
- Minor

nt mutation

- U [N=184]
- C [N=409]

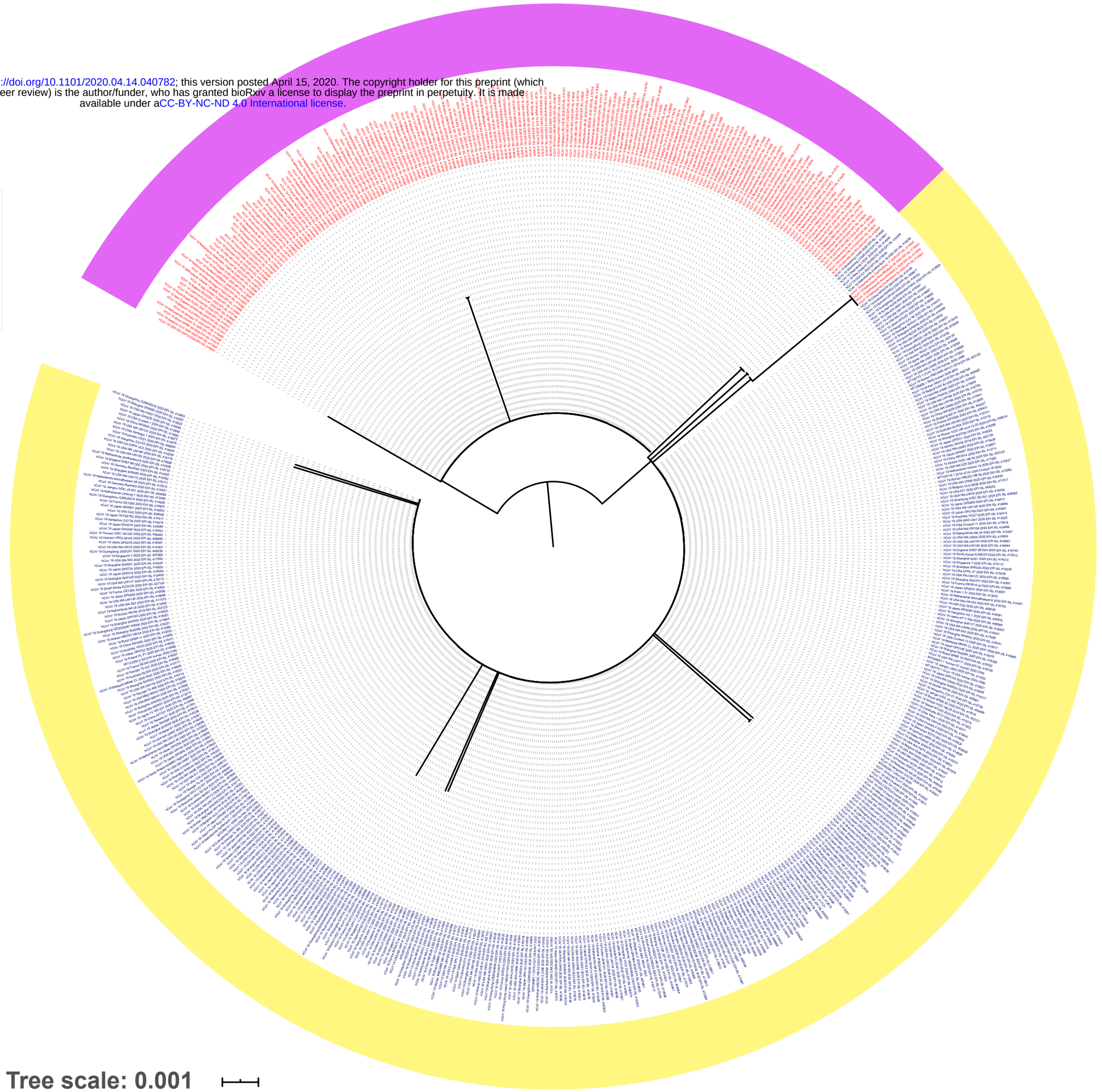

Tree scale: 0.001